Periodic orbits of an almost integrable system

1992 J. Phys. A: Math. Gen. 25 6669

(http://iopscience.iop.org/0305-4470/25/24/019)

J. Phys. A: Math. Gen. **25** (1992) 6669–6683. Printed in the UK

Periodic orbits of an almost integrable system

Sudhir R Jain and H D Parab

Theoretical Physics Division, Central Complex, Fifth floor, Bhabha Atomic Research Center, Bombay 400085, India

Received 12 February 1992, in final form 30 June 1992

Abstract. The aim of this paper is to enumerate and classify all the periodic orbits of the $(\pi/3)$-rhombus billiard. The billiard flow for this system resides on a classically invariant surface of genus two. After transforming the rhombus billiard trajectories on an exactly equivalent set of trajectories on a barrier billiard (with barrier-to-gap ratio equal to 2), we present a criterion facilitating the complete enumeration of periodic billiard trajectories. Having enumerated the trajectories, we classify them distinctly and provide the underlying number-theoretic rationale for the same. Our analysis involves a 'polar construction' which facilitates the determination of lengths of periodic orbits and the areas of the bands in which they occur. It is clear from the analysis that there are no isolated periodic trajectories implying that all the periodic orbits close after an even number of reflections from the boundaries. These results are used to study the family-counting function $F(x)$ (i.e. the number of families of periodic orbits of length less than x) as a function of x.

1. Introduction

Dynamical systems show a wide range of behaviour, from regular (corresponding to exact integrability) to chaotic (pertaining to non-integrability). It is now well understood that integrability of a dynamical system is an exception rather than a rule, and that the generic dynamical system is non-integrable. An immense amount of work has been done towards the improvement of our understanding of classical dynamics of non-integrable systems in the past few decades. The quantum mechanics of these systems, however, is far from clear [1]. It has not been possible to extend semiclassical quantization schemes (e.g. the Einstein–Brillouin–Keller method) which might enable us to sight the first-hand finger-prints of classical chaos in what can be called 'semi-classical chaos'. Alternatively, one can solve the Schrödinger equation with appropriate boundary conditions and study the spectral statistics and the nature of the eigenfunctions, and hence find quantum signatures of classically chaotic features [2, 3]. A disadvantage of this procedure is that it does not allow an easy quantum–classical correspondence unless the Schrödinger equation is solved exactly—a rare occurrence. The most general semiclassical quantization method known today embodies the periodic orbit theory, developed in the late sixties and early seventies by Gutzwiller [4] and Balian and Bloch [5]. In a series of papers, a relation between the solutions of the time-independent Schrödinger equation and the classical periodic orbits was derived. Taking the trace of the Green function over the coordinate space, it was shown that the singularities of the resulting response function give the energy eigenvalues. Moreover, the response function could be written as a sum over all the periodic orbits where each term in the sum contained a phase factor completely determined by the

0305-4470/92/246669+15$07.50

action integral and the Morse index of the orbits, and an amplitude factor determined by the period and the stability exponent of the periodic orbit. The efficacy of this theory has been demonstrated by, for instance, (a) quantization of anisotropic Kepler problem [6] and (b) quantization of the hydrogen atom in a strong magnetic field [7]. Both are examples of completely chaotic systems. It must be pointed out that the enumeration of all the periodic orbits and subsequent determination of action integrals, Morse indices, periods and the stability exponents is an exceedingly difficult task.

In this paper, we deal with a simple pseudointegrable system, the $(\pi/3)$-rhombus billiard. This dynamical system comprises a particle moving inside a $(\pi/3)$-rhombus-shaped box (figure 1) and reflecting from the boundaries in accordance with Snell's law (the angle of incidence equals the angle of reflection). The fact that the system is classically pseudointegrable arises from the existence of two integrals of motion in involution with each other except at the vertices [8]. The set of the trajectories which encounter the vertices has been shown to be of Lebesgue measure zero [9]. Thus the pseudointegrability can be thought of as a step away from integrability, and the question of how this feature manifests itself in the quantal solutions, i.e. the eigenlevel sequences and the eigenfunctions, was posed and answered recently [3]. In summary, the following was shown by solving the Schrödinger equation numerically:

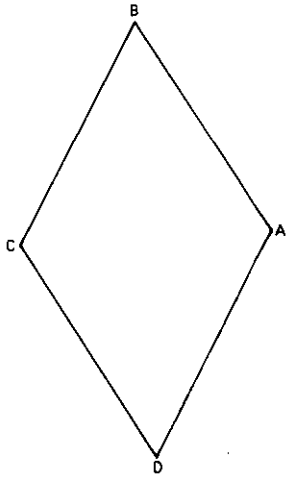

Figure 1. The $(\pi/3)$-rhombus-shaped enclosure in which the particle moves, specularly reflecting from the walls without change in its kinetic energy.

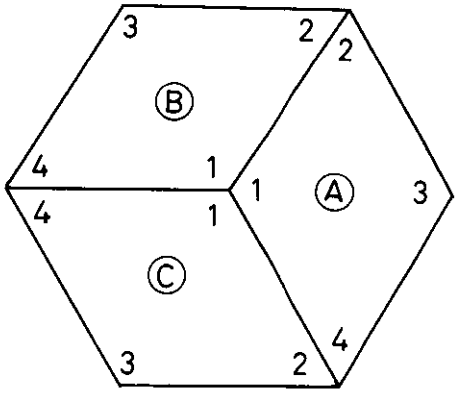

Figure 2. On reflecting the rhombus about a $(2\pi/3)$-vertex, the vertices 1, 2, 3, 4 are seen changing in such a way that on third reflection, we see that 2 and 4 are interchanged.

(i) The nearest-neighbour level spacing statistics agree with the Berry–Robnik distribution [11], having one limit as Poisson distribution (corresponding to integrable systems) and the other as the Wigner surmise (corresponding to chaotic systems). The spectral rigidity also shows an intermediate behaviour in accordance with the classically pseudointegrable behaviour.

(ii) The eigenfunctions non-vanishing on both the diagonals, called pure rhombus modes, show highly irregular behaviour and a Gaussian amplitude distribution, despite the fact that the system has a zero Kolmogorov entropy.

In a beautiful article, the problem of determining the energy spectrum of the $(\pi/3)$-rhombus billiard was tackled by reducing the Schrödinger problem to a set of

functional equations satisfied by some entire functions of a single complex variable having a given asymptotic behaviour [10]. Proceeding in this manner, Gaudin could obtain the first few levels for the $(\pi/3)$-rhombus billiard.

The analysis of the periodic orbits presented here is also of great interest to mathematicians. In mathematical parlance [9], the $(\pi/3)$-rhombus billiard is called almost-integrable, the reasons being the rational ratios of the sides (in this case, trivially, unity) and the internal angles being integral multiples of $\pi/3$. The invariant surface in the phase space is a sphere with two handles, i.e. *genus*, $g=2$. It may be recalled that the invariant surfaces for integrable systems are *tori*, with $g=1$. The subtle difference this makes is that the trajectory in the phase space goes around one of the handles and comes to a point where it has an option of going to any one of the two handles. Mathematically, this idea leads to a shuffling transformation or the interval exchange mapping which is known to be ergodic, even 'weakly mixing'. The possibility of determining the lengths of all the periodic billiard orbits, their Morse indices (related to the number of bounces the orbit suffers before closing) and stability exponents, leads one to successfully employ the periodic orbit theory and obtain the density of states.

In this paper, however, we shall discuss only the classical orbits of the $(\pi/3)$-rhombus billiard. Recent results show that the non-periodic orbits of this system are fractals [18]. Thus, this system possesses bands of periodic orbits in the neighbourhood of which are uncountable fractal trajectories. Gutzwiller periodic orbit theory is developed for the systems where the periodic orbits are unstable and isolated. In the absence of a periodic-orbit sum formula for the orbit-scenario for this system, we leave the semiclassical quantization to a subsequent publication [19], the work being in progress.

In this study, the $(\pi/3)$-rhombus billiard becomes the first non-integrable billiard system for which all the periodic orbits are enumerated, classified and characterized.

We end this introduction by quoting Joseph Ford [12]: '... plane billiards exhibit almost all possible behaviour including chaos, "rational billiards" offer an analytical route to chaos paved with null complexity ... '.

2. Periodic billiard orbits

In the following, we enumerate and classify all the periodic orbits occurring in the $(\pi/3)$-rhombus billiard. Finally, we summarize our results in tabular form.

2.1. Enumeration

To begin with, let us briefly discuss how the motion of a particle inside a $(\pi/3)$-rhombus-shaped enclosure can be visualized as motion on an equivalent barrier billiard, a construction due to Eckhardt *et al* [13]. It is simple to see that after three successive reflections of the rhombus around a vertex of angle $2\pi/3$, the rhombus returns upon itself but with reversed orientation (figure 2). In other words, we obtain the final configuration of vertices as if we have reflected the rhombus about the shorter diagonal of the rhombus joining the vertices 1 and 3. Of course, if we continue the reflections, it will take exactly three more (or equivalently, another reflection about the shorter diagonal) for the rhombus to identify itself with the original orientation. In this picture, due to double-valuedness of the configuration of vertices per direction (by direction,

we mean one of the three directions the rhombus is facing in figure 2), one can visualize three rhombus-orientations in figure 2 on one sheet (or plane) and the subsequent three orientations (required to obtain the original configuration of vertices in rhombus A) on another sheet (or plane). One can visualize a trajectory of particle reflecting from a wall of the rhombus by letting the particle move straight and appropriately reflecting the rhombus about the wall. It is this way of analysing that turns out to be more fruitful and hence the discussion on the tessellation of the plane by rhombi. Due to its equivalence to the Riemann surface of $z^{1/2}$, z being a complex variable, we notice that the two sheets discussed above are joined along straight lines (the complex counterparts are branch cuts) that cannot be crossed; we call these the barriers. Since going to the next plane is to compensate for a phase π, the trajectory must reflect from the barrier.

Alternatively, after three reflections, we can reflect the third rhombus back onto itself (hence compensating for the phase in the first step), i.e. the fourth rhombus comes to lie under the third rhombus. If we continue reflecting now, the sixth rhombus will come to lie under the first rhombus. In this picture, the point 1 in figure 3 will become a (monkey) saddlepoint.

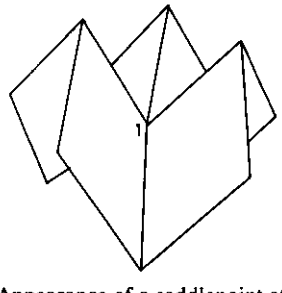

Figure 3. Appearance of a saddlepoint at the vertex 1 in the monkey saddle—a point of negative curvature that repels the particle, hence the cuts in figure 4.

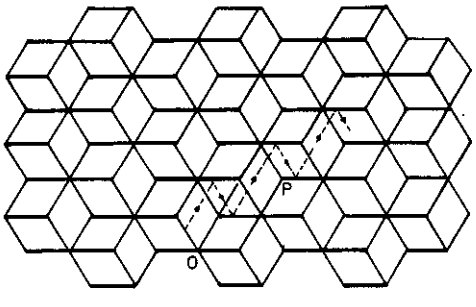

Figure 4. Tessellation of the plane by stacking the fundamental regions (consisting of double hexagons) exploiting the translational symmetry. Barriers are depicted by the bold lines. The point O represents the origin. Owing to the symmetry of the barriers, the integer labelling can be done, e.g. the point P represents a point that can be labelled as $(q, p) = (2, 1)$.

Continuing the process of reflection, we get two planes connected by cuts between the saddlepoints. This construction, projected onto two dimensions, entails an orbit looking like a zig-zag line. We can now construct the fundamental region using six replicas of the rhombus, and subsequently tessellate the two-dimensional plane by stacking the fundamental regions side-by-side, exploiting the translational symmetry. On doing so, we will generate a barrier billiard shown in figure 4 with two sets of planes (call them top and bottom, for instance) interspersed with each other.

Now we concentrate our attention on the barrier billiard where the barrier-to-gap ratio is two. The barrier is comprised of contributions from two rhombi and hence there are two distinguishable sub-barriers giving rise to a single barrier of length twice that of the gap. For a barrier billiard with barrier-to-gap ratio equal to unity, Hannay and McCraw [14] have discussed the classification of periodic orbits. As noted by these authors, their analysis proceeds due to the unit barrier-to-gap ratio, and the

generalizations seem difficult to come by. We now take up our barrier billiard and carry out the analysis leading to the periodic orbits. It must be observed that the barrier billiard corresponding to the rhombus problem is more general than the Hannay–McCraw barrier billiard in two significant ways:

(i) The barrier-to-gap ratio is two, as mentioned above

(ii) the barriers appear in an oblique manner; precisely at an angle of $\pi/3$.

First, we observe that bifurcations of the orbits take place at the two ends of the barrier and at the centre of the barrier. This is due to the fact that each half of the barrier is contributed from two different rhombi in the fundamental region, and the point of bifurcation actually corresponds to a vertex.

The single connected surface is made up of two planes—a top and a bottom. Under the covering of the surface by fundamental regions (double hexagons), the surface thus divides into alternate arrays of both planes containing barriers. Obviously, it does not matter now which plane is called top (or bottom). This argument allows us to choose an origin which, for obvious reasons dictated by symmetry of the barriers, is chosen to be the centre of the barrier, denoted by O in figure 4. Calling the length of a side of the rhombus by L, the barrier length is $2L$ and the gap length is L. On the vertical axis, the perpendicular distance between adjacent arrays of a (top/bottom) plane is $3^{1/2}L$. Since the factor of $3^{1/2}$ is common in the vertical axis, we choose to measure the length in this direction in terms of $3^{1/2}$, thereby making the ordered pairs, labelling the points, purely consisting of integers, (q, p). For instance, a point P will be labelled by (2, 1) (figure 4).

A typical trajectory on this surface will be made up of alternate motions in the top and the bottom planes. Since every plane consists of an identical array of barriers, the trajectory starting at an angle with the plane from an initial point and ending on an equivalent point on the same plane constitutes a periodic orbit (see, for example, figure 5). Instead of following the zig-zag path, we can unfold the trajectory into an exactly equivalent straightened version. Subsequently, we must decide which directions lead to periodic orbits.

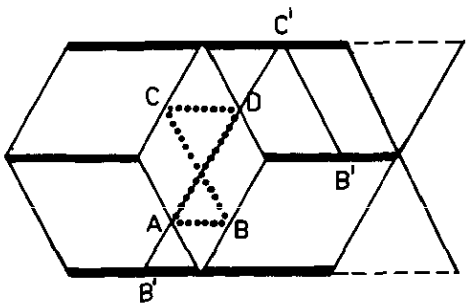

Figure 5. Equivalent to a periodic orbit in the rhombus BADCB, we see here a periodic orbit in the barrier billiard B'ADC'B'. It may be noted that the orbit in the barrier billiard closes at an equivalent point on the other plane.

By virtue of the integer labelling, it is clear that all those directions that end on an (integer, integer) ordered pair correspond to periodic orbits. Leaving apart a factor of $3^{1/2}$ in the vertical direction, these directions correspond to rational gradients on each (bottom or top) plane. Also, starting from the origin, we must consider only those

endpoints such that q and p are coprime to avoid overcounting. By the symmetry of the barriers on the plane, we must restrict ourselves to the upper-half region only. Further, taking care of the geometry of our system, we must apply the restriction that either $p \leq q$ or $q \leq 3p$ $(q, p = 0)$. Obviously then three classes emerge, namely (q, p) can be (i) (odd, odd), or (ii) (odd, even), or (iii) (even, odd). Next, we have to classify the number of bands or families of periodic orbits that correspond to each direction. Before undertaking this we need to convince ourselves that there can be no more periodic orbits then those obtained in the manner described above.

For equal barrier-to-gap ratio, it was shown that any trajectory with an irrational gradient can be approximated arbitrarily well by trajectories with rational gradients, utilizing Klein's string construction or the continued fraction expansion. However, those trajectories never close in both position and momentum; rather they form a curious zig-zag. This zig-zag path, for quadratic irrational gradients, has a fractal dimension. For the barrier billiard in our case, the same holds [18]. Hence, we conclude that the trajectories with any irrational gradient do not close.

It, therefore, follows that if we take into account all the rational gradients, avoid overcounting and classify different families/bands, we will have enumerated all the periodic orbits.

For further analysis we resort to an alternative construction for reasons of clarity and easy generalization, and name it the polar construction.

2.1.1. Polar construction. Exploiting the periodicity of the barrier-gap-barrier-gap-... string, we wrap the basic string on two circles representing two different planes. Each circle has three basic divisions, coming out of two barriers (from two rhombi, joined together) and a gap. Each division now corresponds to an angle of $2\pi/3$. The skew manner in which the barriers on both planes are stacked is accounted for here by giving an appropriate phase difference between equivalent points on two circles (see, e.g. figure 6). A (q, p) direction can be represented on these circles by the following procedure.

Divide each segment of the inner circle (only for the sake of clarity, it may as well be the outer one) into p parts after fixing the origin at the point joining the two

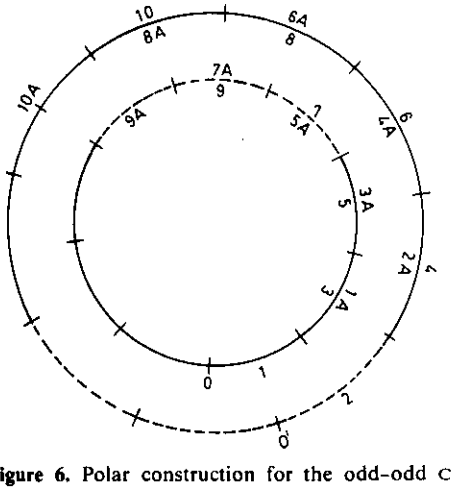

Figure 6. Polar construction for the odd-odd CE case. The typical case for which the diagram is drawn is $(q, p) = (1, 3)$.

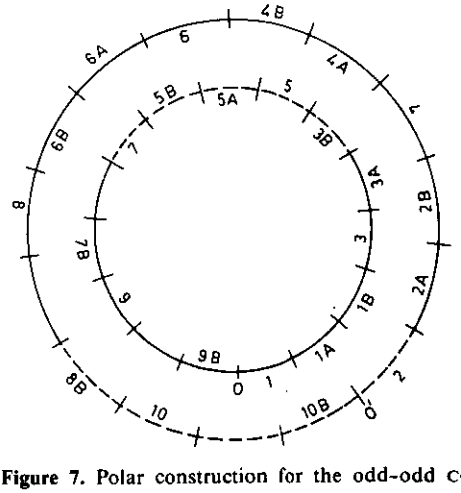

Figure 7. Polar construction for the odd-odd CC case. The typical case for which the diagram is drawn is $(q, p) = (3, 5)$.

sub-barrier segments. The origin of the outer circle will be at an angle of $\pi q/3p$ from the origin of the inner circle (moving along the circular arc in a definite sense, taken anticlockwise here). After fixing the origin, the outer circle has to be divided into $3p$ parts of equal length with one division at the origin. Since there are two gradients, positive and negative, we adopt the convention of marking outside (inside) the circle as a representative of positive (negative) gradient.

To follow a trajectory, we start with an arbitrary point on one of the p subsegments of the barrier segment to the right of the origin, on the inner circle. The next point will be on the outer circle at the same distance (= number of subsegments) from the origin of the outer circle as the previous point was from its respective origin. As is clear from earlier discussion, these points must alter between the outer and the inner circles. The following point comes on the inner circle but q subsegments away from the original one, and the next on the outer circle q subsegments away from the previous one, and so on. Going on in this way, after a finite number of points, we will reach the starting point on the inner circle and that would make one periodic orbit. Although this is generally valid, in some cases it may not lead to the minimal length of the orbit. Such would be the case when, after exactly half the number of reflections, the trajectory closes, i.e. reaches a point corresponding to the same respective subsegment as it started with, on the outer circle. At first sight, it might seem erroneous to consider this as a periodic orbit. However, to resolve this point, the following may be recalled: the procedure of erecting barriers and subsequent polar construction leads to an easy classification of orbits; however, a more fundamental idea is the straightening of a trajectory, reflecting the domain about the edge on which the particle is incident. For the cases where the length of an orbit turns out to be double by the polar construction, one can easily see that, using the 'domain-reflection method', one gets the correct length. Thus, without ambiguity, the trajectory in the polar construction must be considered periodic even if it seems to be closing on the other plane (see, for example, the illustration in figure 5). With this clarification, we need only think in terms of the polar construction. Different sequences of barriers and gaps correspond to different orbits. It is quite clear that all the orbits occur in bands.

2.2. Classification

As we have seen above, the most elementary classification is in (q, p) being (odd, odd), (odd, even) and (even, odd). Having set the origin at the centre of the barrier, the trajectory sets off in some rational direction and reaches either the centre or an end (left or right) of a barrier. It is rather obvious to see that for each of the three cases above, there are subclasses which we shall call the centre-to-centre (CC) case and the centre-to-edge (CE) case. Our procedure of classification uses the following steps:

(i) using the polar construction, we depict the trajectory on the circles with an opening and an ending point on one of the subsegments of a segment. We go on to other subsegments of the same segment, exploring the positive and the negative gradients until both sides of the circles are filled. In all, we must fill $12p$ points;

(ii) check if the orbit has already closed half-way on the outer circle, or equivalently, on the other plane.

With these steps in mind, we now take up each class separately and classify the bands of periodic orbits in full.

Case 1: odd-odd CE. We first describe, through a simple example, how we can arrive at general conclusions. Our approach is to make a conclusion based on empirical data

obtained by 'brute force'. Finally we will provide a rationale supporting and explaining the conclusion obtained.

Let us consider the case of $(q, p) = (1, 3)$. The corresponding polar construction is shown in figure 6. As can be seen, point 1 and point 10 identify with each other, forming a periodic orbit after six bounces. Also, there is an orbit with negative gradient. It should be noted that all the subsegments are visited by just these two orbits. The orbits close half-way on $(3q, 3p)$, on the other plane, and there are two bands of orbits.

Drawing the polar construction for other odd-odd CE cases, it can be seen that there are only two bands of orbits as seen above.

Now we come to discuss the rationale behind this classification of orbits. Due to the polar construction, each subsegment is an arc of angle $2\pi/3p$. Translating the formation of periodic orbit by the polar construction into an equation, we trivially get

$$N(2\pi/3p)q = 2\pi M \tag{1}$$

where N denotes the number of subsegments and M denotes the number of rotations by 2π. Henceforth, we will call N the 'crossing index' and M the 'rotation number'. Equation (1) is simply

$$Nq = 3Mp \tag{1a}$$

where M, N, q, p are positive integers. Since this is a CE case, q is not a multiple of three, i.e. $q = 3l$, $l \in \mathbb{Z}$. Thus, the only way in which equation (1a) can be satisfied is if $q = M$ and $3p = N$. Note that M and N will be odd as both q and p are odd. The crossing-index on one circle is $3p$ implying that the total crossing-index is $6p$ after which the orbit closes. In all, there are $12p$ subsegments and hence there are exactly two bands of periodic orbits.

In general, the crossing-index is given by [15]

$$N = [q, 3p]/q \tag{2}$$

and the rotation number is given by

$$M = [q, 3p]/3p \tag{3}$$

where $[a, b]$ denotes the lowest common multiple of a and b. Trivially, for the CE case, $N = 3p$ and $M = q$; for the CC case, $N = p$ and $M = q/3$.

Case 2: odd–odd CC. Firstly, all the rational directions pointing towards an infinite number of avenues correspond to the bands of periodic orbits. Points (q, p) corresponding to avenues are of the form $(3(2k-1), 1)$, $k \in \mathbb{Z}$. For each direction there are two bands corresponding to positive and negative gradients.

We go over to a representative of a general case, namely $(q, p) = (3, 5)$. The polar construction is depicted in figure 7. There are three strings of points corresponding to three bands of periodic orbits. Including the opposite gradients, there are four distinct bands in all. The string starting with point 1 and ending with point 11 closes after six reflections. The case for 1B–11B orbit is the same. The opposite gradient counterpart of 1–11 (1B–11B) is equivalent to itself, starting from the outer circle (at 6 (6B)). So these strings give us two bands of periodic orbits. Care must be taken for the periodic orbit starting with the point 1A. The orbit closes at 6A as this is the subsegment corresponding to 1A on the inner circle and the gradient matches. The orbit 1A-6A closes after four reflections and occurs in a band. Taking the opposite gradient, we get two bands of periodic orbits here.

For other odd-odd CC cases, we obtain the same results as in the above-mentioned case. Let us now see the reason for the occurrence of four bands of periodic orbits in this case.

From equations (2) and (3), $M = q/3$ and $N = p$. For each orbit, the crossing-index will be $2p$ accounting for the other circle also. In total, there are $12p$ segments and it clearly follows that there must be six bands of periodic orbits. Subtracting the two equivalent bands, we are left with four bands.

Case 3: odd-even CE. Consider $(q, p) = (1, 2)$. The polar construction is drawn in figure 8. There is a bifurcation in the band of trajectories starting with point 1, and further continuing with two bands, primed and unprimed, to eventually close at 13′ and 13 respectively. This feature, which can be succinctly described as bifurcation of the vector fields at vertices and continuation of trajectories in the form of bands (a signature of zero Lyapunov exponent) is typical of pseudointegrable systems. The points 1 and 6′ are, indeed, identical. Orbits emanating from 1 and 6′ (1A and 6A′) will be the same. Consequently, on allowing the opposite gradients, we get just two bands of periodic orbits.

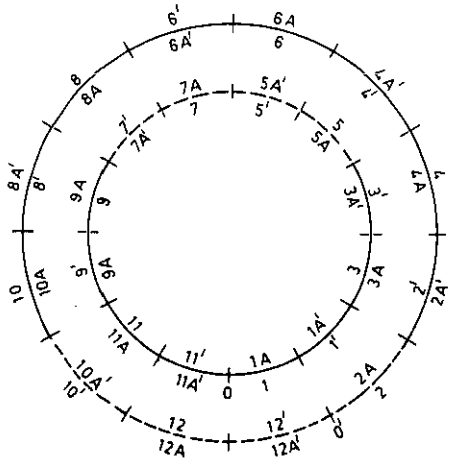

Figure 8. Polar construction for the odd-even CE case. The typical case for which the diagram is drawn is $(q, p) = (1, 2)$.

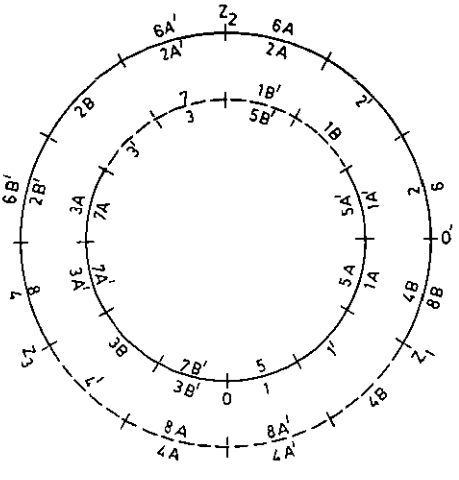

Figure 9. Polar construction for the odd-even CC case. The typical case for which the diagram is drawn is $(q, p) = (3, 2)$.

All other examples of this class give rise to the same number of bands and the orbit types are also similar. Of course, the lengths and other details will be different.

As the arguments for justification follow the same lines, we will not repeat them for this and further cases.

Case 4: odd-even CC. For this case, consider $(q, p) = (3, 2)$, the polar construction for which is drawn in figure 9. Due to bifurcations, we have drawn double the marks, thus, making explicit that we have to fill $24p$ points in all. As can be seen from the diagram, there are four bands of periodic orbits: an orbit corresponding to the string 1 2 . . . 9; another orbit corresponding to the string 1A 2A . . . 9A; and a positive-negative gradient pair 1′ 2′ . . . 5′ (plus the opposite gradient). It is interesting to see that bifurcations of these vector fields take place at all possible places, namely Z_1, Z_2 and Z_3.

Considering other odd-even cases, one can easily see that the same conclusions about the number of bands, etc, will hold, leaving apart the finer details.

Case 5: even-odd CE. Consider $(q, p) = (2, 1)$, the polar construction for which is shown in figure 10. There are two bands of periodic orbits. In fact, the periodic orbit formed with opening point as the negative-gradient-equivalent of the point 1 is identical to the orbit 1A 2A ... 7A, starting from 2A. Thence, the string 1 2 ... 7 and its negative gradient counterpart are the two bands in this case.

Case 6: even-odd CC. A general case can be studied through the example of $(q, p) = (6, 5)$, the polar construction being depicted in figure 11. Although the diagram is

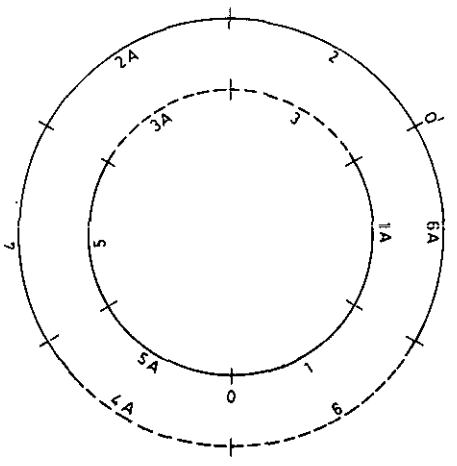

Figure 10. Polar construction for the even-odd CE case. The typical case for which the diagram is drawn is $(q, p) = (2, 1)$.

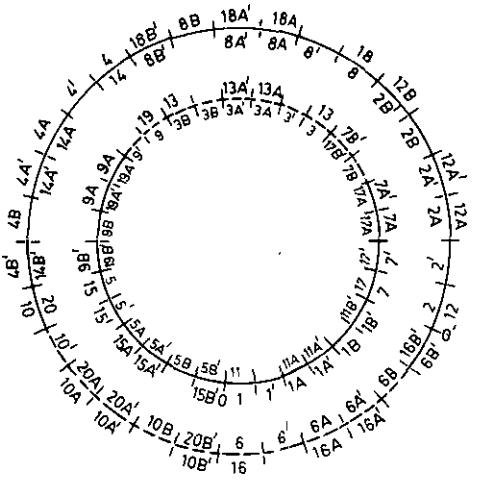

Figure 11. Polar construction for the even-odd CC case. The typical case for which the diagram is drawn is $(q, p) = (6, 5)$.

Table 1. Summary of the results obtained for the periodic orbits in section 2. In column 3, 1-1 stands for one positive and one negative gradient periodic orbit. In column 4, $(q/2, p/2)$ indicates the fact that the orbit closes a half-way of (q, p). The symbol $f_{qp} = (q^2+3p^2)^{1/2}$ and L is the sidelength of the rhombus.

Type	Classes	No. of families	Closing point	Length of the orbits	Area of the band
Centre-centre					
	odd-odd	1-1	$(q/2, p/2)$	$Lf_{qp}/2$	$\frac{1}{2}\sqrt{3}/L^2$
		2	(q, p)	Lf_{qp}	$\sqrt{3}L^2$
	odd-even	1-1	(q, p)	Lf_{qp}	$\frac{1}{2}\sqrt{3}/L^2$
		2	$(2q, 2p)$	$2Lf_{qp}$	$\sqrt{3}L^2$
	even-odd	1-1	(q, p)	Lf_{qp}	$\frac{1}{2}\sqrt{3}/L^2$
		2	$(2q, 2p)$	$2Lf_{qp}$	$\sqrt{3}L^2$
Centre-edge					
	odd-odd	1-1	$(3q/2, 3p/2)$	$3Lf_{qp}/2$	$\frac{1}{2}\sqrt{3}/L^2$
	odd-even	1-1	$(3q, 3p)$	$3Lf_{qp}$	$\frac{1}{2}\sqrt{3}/L^2$
	even-odd	1-1	$(3q, 3p)$	$3Lf_{qp}$	$\frac{1}{2}\sqrt{3}/L^2$

getting rather complicated, in the same manner as discussed earlier, it can be concluded that there are four bands of periodic orbits. The general validity of this conclusion can be verified without undue hardship.

The results of this section, along with the lengths of the periodic orbits and the phase space areas of the bands in which they occur, are summarized in table 1.

3. Distribution of periodic orbits

The results of section 2 clearly show that there are a countable number of families of periodic orbits. By family of periodic orbit we mean an isolated trajectory closing after an odd number of reflections, or a band of trajectories closing after an even number of reflections. We have also seen that the periodic trajectories only occur in bands for the $(\pi/3)$-rhombus billiard due to its equivalence with the barrier billiard discussed in the last section. The number of families of periodic orbits less then x is finite for any x [9]. We call this number by the counting function, $F(x)$. In this section, we study $F(x)$ in the light of the results obtained in section 2.

For a polygon, it is conjectured [16] that

$$F(x) = cx^n + O(x^{n-1}). \tag{4}$$

For almost-integrable polygons (the $(\pi/3)$-rhombus being one such case), $n = 2$. First, we paraphrase a theorem due to Gutkin [9].

Theorem. Let P be an almost-integrable polygon and let Δ be the corresponding integrable one. Let g be the genus of the surface R corresponding to P. Denote by $|P|, |\Delta|$ the areas of P and Δ respectively. Then there is a constant c_1 depending on P, $1 \leqslant c_1 \leqslant |P|/|\Delta|$, such that

$$F(x) = c_1 \pi g x^2/|P| + O(x). \tag{5}$$

We now present number-theoretic arguments to obtain $F(x)$ for our case. Subsequently, we shall discuss and compare our results with the above-mentioned results by Katok and Gutkin. The length of periodic orbits in the given family corresponding to the lattice point (q, p), where q, p are coprime, is given by $l = c_2 L(q^2 + 3p^2)^{1/2}$ where c_2 depends on the family of periodic orbits as seen in table 1. If $l \leqslant x$ for a given family of points (q, p) the contribution from this family of (q, p) should be counted in $F(x)$. We can draw a circle of radius l_1 $(= q_0 L)$, then, all points (q, p) having family of periodic orbit with length $c_2 l_1 \leqslant x$ (or $l_1 \leqslant x/c_2$) should be considered for the calculation of $F(x)$. Referring to figure 12, the area of a quarter circle is $\pi l_1^2/4$ and the area of the square OABC is l_1^2. We shall denote the integer (fractional) part of a number by $[\ldots]$ $(\{\ldots\})$. The number of lattice points in OABC is

$$N = (q_0+1)[(q_0+1)/\sqrt{3}] = (q_0+1)^2/\sqrt{3} - (q_0+1)[(q_0+1)/\sqrt{3}].$$

On average, $[(q_0+1)/\sqrt{3}]$ is $\frac{1}{2}$ (obviously); hence

$$N \sim q_0^2/\sqrt{3} + (2q_0+1)/\sqrt{3} - (q_0+1)/2.$$

Therefore, the number of lattice points in a quarter circle is

$$N_q = N(\pi l_1^2/4)/l_1^2 = \pi N/4.$$

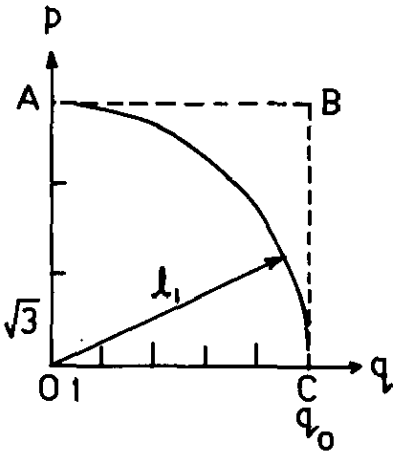

Figure 12. See text.

Since the probability that two randomly chosen numbers are coprime is $6/\pi^2$ [15], the number of coprime lattice points is

$$N_c = (6/\pi^2)(\pi N/4) \sim (\sqrt{3}l_1^2/2\pi L) + A\sqrt{3}/4\pi \qquad (\text{since} \quad q_0 = l_1/L, \quad L = \text{sidelength})$$

where $A = (4-\sqrt{3})l_1/L + 2 - \sqrt{3}$.

For reasons discussed in the previous sections, we are concerned with finding the number of points in a $\pi/3$-sector, the area of which is two-thirds that of a quarter circle. Hence, for a $(\pi/3)$-sector

$$N'(l_1) \sim l_1^2/\sqrt{3}\pi L^2 + A/2\sqrt{3}\pi.$$

Taking only the dominant contribution ($O(l_1^2)$), with the help of table 1, we can write for the number of periodic orbits whose length is $\leqslant x$

$$\begin{aligned} F(x) \sim 2(&P_{oocc}N_{oocc}(2x) + P_{oocc}N_{oocc}(x) + P_{oecc}N_{oecc}(x) \\ &+ P_{oecc}N_{oecc}(x/2) + P_{eocc}N_{eocc}(x) + P_{eocc}N_{eocc}(x/2) + P_{ooce}N_{ooce}(2x/3) \\ &+ P_{oece}N_{oece}(x/3) + P_{eoce}N_{eoce}(x/3)) \end{aligned}$$

where P_{oocc} is the probability that given coprime lattice point is of odd-odd, centre-centre type, and so on, $N_{oocc}(l)$ is total number of odd-odd, centre-centre type coprime lattice points contained in the sector. Out of four points only one is odd-odd (or even-odd or odd-even), also two out of three points are of centre-edge type and one is of centre-centre type. Therefore we have

$$P_{oocc} = P_{oecc} = P_{eocc} = \tfrac{1}{9} \tag{6}$$

$$P_{ooce} = P_{oece} = P_{eoce} = \tfrac{2}{9}. \tag{7}$$

Thus we can write

$$\begin{aligned} F(x) &= 2((4+1+1+\tfrac{1}{4}+1+\tfrac{1}{4})(x^2/9\sqrt{3}\pi L^2) + (\tfrac{4}{9}+\tfrac{1}{9}+\tfrac{1}{9})(2x^2/9\sqrt{3}\pi L^2)) \\ &= [53/(27\sqrt{3}\pi L^2)]x^2 \\ &= 0.082\,24x^2 \end{aligned}$$

or

$$\simeq 0.049\,733(2\pi/|P|)x^2. \tag{9}$$

Of course, apart from the dominant term that is quadratic in x, there will be terms of $O(x)$ and $O(1)$. It is, however, important to note here that term of $O(x)$ is not related to the orbits periodic after an odd number of reflections (hence, isolated). These terms only present a more exact expression for $F(x)$ arising from the above arguments. Their origin is in the points contributing to $F(x)$ lying on the boundary of the sector. On the same lines as above, terms of $O(x)$ and $O(1)$ are found to be $(26/81\pi)(4\sqrt{3}-3)(x/L)$ and $(12/27\pi)(2\sqrt{3}-3)$ respectively.

One can see from figure 13 that the number-theoretic estimate is an asymptote to the numerically obtained result (based on section 2). Even for $x<10^2$, one sees a quadratic law. The fast asymptotic convergence to the quadratic law is mainly because of fast asymptotic convergence of the coprime probability law $(6/\pi^2)$ used above. Thus, the asymptotic law of proliferation of periodic orbits in the $(\pi/3)$-rhombus billiard is, indeed, exactly quadratic. This establishes and extends Katok's conjecture stated earlier. However, our result does not agree with the prefactor in the Gutkin theorem. The constant c_1 (in the theorem) as seen by our analysis is $53/108\pi^2$ (roughly 0.05). But, c_1 is greater than or equal to 1 in the statement of the theorem. This disagreement is mainly due to the following reason. In considering the number of points on the lattice formed by the fundamental regions of the corresponding integrable system, the fact that any pair of numbers (q', p') (a multiple of some coprime (q, p)) cannot be distinguished from (q, p) was not taken into account. Thus, once the contribution to $F(x)$ is considered for a coprime pair (q, p), no more (although there are countably infinite) multiples thereof need consideration. Further, since only a $(\pi/3)$-sector is required for the complete calculation, c_1 will reduce by another factor of 1/6. Finally, notice that there is a basic difference between the lattice generated by

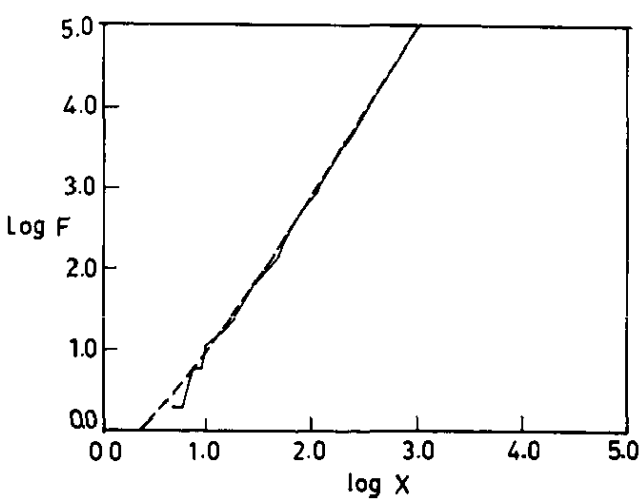

Figure 13. A log–log plot of the counting function, $F(x)$, versus the length of the periodic orbit, x. The broken curve represents the estimate derived in section 3 ($0.082\,24x^2+0.191\,63x+0.065\,656$) and is compared with the full curve obtained from the results of section 2. It can be seen that an exact quadratic law holds after x approximately exceeds 40 units. Below this, the dependence is a combination of quadratic and linear behaviours.

fundamental regions of the $(\pi/3)$-rhombus billiard and its corresponding integrable system (equilateral triangle) and that is in the incomplete tessellation of the plane resulting in uncovered regions manifested in zero-width, finite-length barriers. It is this structure that enables us to complete the classification via integer-labelling. Of course, it matters whether (q, p) is (odd, odd), (odd, even) or (even, odd) as can be verified from table 1. A look at the analysis presented earlier in this section reveals that in this case (at least), the prefactor must reduce further by another order. Hence, the bounds on c_1 given by Gutkin are not correct (although the quadratic part of the law is correct) inasmuch as, at least the lower bound has to reduce to $O(10^{-2})$ (in agreement with our calculation, $53/108\pi^2$).

4. Discussion

Before discussing our results, let us summarize them. The $(\pi/3)$-rhombus billiard was mapped onto an equivalent barrier billiard on two two-dimensional planes. Due to periodic occurrence of the barriers, an appropriate integer labelling was facilitated which, in turn, allowed us to present a simple criterion for the enumeration of periodic orbits. For classification of orbits, we exploited the translational symmetry thereby allowing us to develop a 'polar construction' of the barrier–gap geometry. Owing to the compactness of the construction, we were able to classify the periodic orbits. Indeed, the polar construction provides a code for the periodic orbits of this system. These results were used to obtain the family counting function. We also developed a probabilistic number theoretic argument to explain the family counting function, subsequently discussing our results in the light of some of the earlier results. More precisely, it was shown that the periodic orbits proliferate in accordance with a quadratic power law as compared to the exponential law for the chaotic systems.

Our analysis can be easily generalized to enumerate orbits for any other barrier billiard with a rational barrier-to-gap ratio. For other oblique angles also, the analysis is possible to extend itself by taking care of the phases in an appropriate manner.

Although the $(\pi/3)$-rhombus billiard is an example of almost integrable billiards (in general, pseudointegrable systems), it must be emphasized that it is a non-integrable system. A study of quantal-classical correspondence, very important for non-integrable systems, necessitates semiclassical results. Indeed, the only semiclassical theory valid for all systems is the periodic orbit theory. The periodic orbit theory developed by Gutzwiller has been shown to yield very good results when the system is completely chaotic and integrable. The systems on which the theory has been tested are the ones with all the periodic orbits unstable and isolated. Here, we have a system wherein all the periodic orbits occur in bands (hence, the Morse indices are (number of reflections before closure) times π). Also, very recent results show that all the non-periodic orbits are very complicated fractal trajectories [18]. As mentioned in the introduction, it follows from our work that to understand the semiclassical quantization of this system (typical of this class of systems), one needs to develop a periodic orbit theory with the orbit-scenario discussed above.

There are two well known difficulties in the periodic orbit theory:

(i) it is extremely difficult to enumerate and classify the periodic orbits, determine the lengths and stability parameters; and

(ii) the periodic orbit sum is, at best, conditionally convergent; generally, it is divergent and it has not been possible to resum it in a meaningful manner [17].

In this paper, we have been successful in overcoming the first hurdle. As far as the second one is concerned, in the light of the recent results [18], work is in progress [19].

References

[1] Eckhardt B 1988 *Phys. Rep.* **163** 205
[2] McDonald S W and Kaufman A N 1988 *Phys. Rev.* A **37** 3067
[3] Biswas D and Jain S R 1990 *Phys. Rev.* A **42** 3170
[4] Gutzwiller M C 1967 *J. Math. Phys.* **8** 1979; 1969 *J. Math. Phys.* **10** 1004; 1970 *J. Math. Phys.* **11** 1791; 1971 *J. Math. Phys.* **12** 343
[5] Balian R and Bloch C 1974 *Ann. Phys.* **60** 401
[6] Gutzwiller M C 1982 *Physica* **5D** 183
[7] Wintgen D 1988 *Phys. Rev. Lett.* **61** 1803
[8] Zemlyakov A N and Katok A 1976 *Math. Notes* **18** 760
[9] Gutkin E 1986 *Physica* **19D** 311
[10] Gaudin M 1987 *J. Physique* **48** 1633
[11] Berry M V 1983 *Chaotic Behaviour of Deterministic Systems. (Proc. Les Houches Summer School, Session XXXVI)* ed G Iooss, R H G Helleman and R Stora (Amsterdam: North-Holland) p 252
[12] Ford J 1986 *Chaotic Dynamics and Fractals* ed M F Barnsley and S G Demko (London: Academic) p 36
[13] Eckhardt B, Ford J and Vivaldi F 1984 *Physica* **13D** 339
[14] Hannay J H and McCraw R J 1990 *J. Phys. A: Math. Gen.* **23** 887
[15] Schroeder M R 1984 *Number Theory in Science and Communication* (Berlin: Springer-Verlag) 2nd edn, p 18
[16] Katok A 1986 The growth rate for the number of saddle connections for a polygonal billiard *Preprint*
[17] Cvitanovic P and Eckhardt B 1989 *Phys. Rev. Lett.* **63** 823
[18] Jain S R and Pandey A 1992 in preparation
[19] Jain S R and Parab H D 1992 in preparation